Obrabotka metallov (tekhnologiya, oborudovanie, instrumenty) = Metal Working and Material Science. 2026 vol. 28 no. 2 pp. 179–195
ISSN: 1994-6309 (print) / 2541-819X (online)
DOI: 10.17212/1994-6309-2026-28.2-179-195

NSTU NETI

Obrabotka metallov -
Metal Working and Material Science

Journal homepage: http://journals.nstu.ru/obrabotka_metallov

Ultrasonic non-destructive property prediction framework for spheroidal graphite iron castings

Digvijay Mhamane [1, a,*], ***Anand Bewoor*** [2, b]

[1] Department of Mechanical Engineering, Zeal College of Engineering and Research, Narhe Pune, Savitribai Phule Pune University, Pune – 411041, Maharashtra, India

[2] Cummins College of Engineering for Women, Pune – 411052, Maharashtra, India

[a] https://orcid.org/0000-0002-3277-0443, digvijay.ndt@gmail.com; [b] https://orcid.org/0000-0001-9329-3807, anand.bewoor@cumminscollege.in

ARTICLE INFO

Article history:
Received: 22 February 2026
Revised: 27 February 2026
Accepted: 11 April 2026
Available online: 15 June 2026

Keywords:
Spheroidal graphite iron
Non-destructive testing
Ultrasonic velocity
Property prediction

ABSTRACT

Introduction. Spheroidal graphite (*SG*) iron is widely used in engineering structures due to its high mechanical properties, which are largely determined by the degree of spheroidization (nodularity) of the graphite inclusions. Conventional metallographic evaluation of nodularity provides high accuracy but is a destructive and time-consuming procedure. Therefore, there is a need for a reliable non-destructive approach for rapid quality assessment of castings, especially in small-batch foundry production. ***The purpose of this work*** is to develop a methodological framework for predicting nodularity and mechanical properties of *SG* iron castings based on ultrasonic testing. **Methods.** Castings of three *SG* iron grades (*SGI 400/12*, *500/7*, and *600/3*) were manufactured according to a *Taguchi L27* experimental design. The controlled process parameters were: pouring temperature (1,380–1,420 °C), carbon equivalent (4.0–4.6), and section thickness (5–15 mm). Ultrasonic testing was performed using a flaw detector with a 4 MHz transducer to measure the longitudinal ultrasonic wave velocity in the samples. Nodularity was determined from the ultrasonic measurements using the instrument's internal calibration and the corresponding velocity relationship. Ultimate tensile strength (*UTS*, σ_u) and *Brinell* hardness were determined by standard mechanical testing methods. Multiple linear regression models were developed relating the process parameters and ultrasonic velocity to nodularity, *UTS* (σ_u), and hardness. **Results and Discussion.** The developed models demonstrated high predictive capability, with coefficients of determination of R^2 = 0.8955 for nodularity, R^2 = 0.9954 for *UTS* (σ_u), and R^2 = 0.8135 for hardness. Carbon equivalent was identified as the most significant parameter affecting all responses. Ultrasonic velocity showed a clear positive correlation with nodularity and mechanical properties. Validation using metallographic analysis confirmed good agreement with ultrasonic predictions, with deviations within 2–3%. The study demonstrates that ultrasonic velocity can be effectively used to predict the microstructural and mechanical characteristics of *SG* iron. The developed regression models provide a simple and practical tool for non-destructive evaluation, ensuring rapid quality control in foundry production, especially for small-scale enterprises.

For citation: Mhamane D., Bewoor A. Ultrasonic non-destructive property prediction framework for spheroidal graphite iron castings. *Obrabotka metallov (tekhnologiya, oborudovanie, instrumenty) = Metal Working and Material Science*, 2026, vol. 28, no. 2, pp. 179–195. DOI: 10.17212/1994-6309-2026-28.2-179-195. (In Russian).

Introduction

Spheroidal graphite iron (*SG* iron), also known as ductile iron, is widely used in automotive, machinery, and structural components because it provides a good balance of strength, ductility, wear resistance, and castability [1–4]. The mechanical performance of *SG* iron mainly depends on the shape, size, and distribution of graphite nodules present in the microstructure. Higher nodularity generally improves tensile strength, ductility, and fatigue resistance, whereas irregular graphite shapes may reduce the mechanical performance

*** Corresponding author**
Mhamane Digvijay, Research Scholar
Department of Mechanical Engineering,
Zeal College of Engineering and Research, Narhe Pune,
Savitribai Phule Pune University,
411041, Pune, Maharashtra, India
Tel.: 0230 242 1300, **e-mail:** digvijay.ndt@gmail.com

of cast components. Therefore, reliable evaluation of nodularity and microstructure is critically important in foundry production and quality control.

Conventionally, nodularity and microstructural characteristics are evaluated using metallographic examination. This method requires sectioning, polishing, and microscopic observation of samples. Although metallography provides accurate results, it is destructive and time-consuming for real-time monitoring during manufacturing. Because of these limitations, researchers have explored various non-destructive testing (*NDT*) techniques to evaluate the microstructure and mechanical properties of cast irons without damaging the component [5–6]. Ultrasonic velocity measurement offers a non-destructive alternative, enabling rapid, objective assessment without material waste [5–6].

Ultrasonic testing has been extensively studied for material characterization among the various *NDT* methods. Grain boundaries, inclusions, and graphite nodules are examples of internal features that ultrasonic waves can interact with as they travel through solids. Since the propagation behavior of ultrasonic waves depends on the elastic properties and internal structure of the material, parameters such as ultrasonic velocity and attenuation can provide crucial information regarding microstructure and mechanical properties. Because ultrasonic waves can pass through materials and be detected by ultrasonic equipment, physical properties, including a material's elasticity, can be evaluated. To assess the mechanical and microstructural properties of materials in practical situations, a variety of ultrasonic measurement methods and instruments have been developed [7]. It is noteworthy that most researchers have used ultrasonic velocity and attenuation data to correlate ultrasonic measurements with microstructure and mechanical behavior.

In practice, ultrasonic techniques have been successfully used for a variety of material characterization tasks. These involve determining the bulk modulus, shear modulus, *Young's* modulus, and other elastic constants of metals [8–9]. Ultrasonic methods have also been used to assess microstructural characteristics, such as grain size and its growth during processing [10]. Additionally, ultrasonic data can be used to evaluate mechanical parameters such as hardness [11] and yield strength [12]. Furthermore, researchers have used ultrasonic techniques to monitor processing parameters, such as recrystallization during heat treatment and the depth of hardened layers in surface-treated components [13]. These features have made ultrasonic testing one of the most widely used *NDT* methods in the engineering sector.

Ultrasonic inspection techniques have become more capable in recent years due to a number of technological advancements. *Phased Array Ultrasonic Testing* (*PAUT*), *Time-of-Flight Diffraction* (*TOFD*), *Full Matrix Capture* (*FMC*), and *Automated Ultrasonic Testing* (*AUT*) are examples of advanced techniques that enhance flaw detection, internal defect imaging, and automated inspection of complicated geometries [14]. These developments make it possible to characterize internal structures and flaws in engineered materials with greater accuracy.

Other non-destructive techniques for assessing nodularity in cast irons have been studied in addition to ultrasonic testing. Electromagnetic methods, such as eddy current testing, detect changes in magnetic and electrical conductivity brought on by microstructural alterations. Similarly, resonance techniques measure the natural vibration frequency of a component in order to evaluate its elastic properties. While these approaches are useful, ultrasonic techniques are better suited for foundry applications because they are easier to implement for thick castings and often have a higher sensitivity to internal microstructural changes [15–16].

Researchers have linked ultrasonic parameters to microstructure and mechanical properties using statistical modeling tools in addition to experimental techniques. Regression models are frequently employed to establish relationships between ultrasonic velocity and characteristics including hardness, tensile strength, and nodularity. In recent years, machine learning techniques have been used to improve prediction accuracy by concurrently evaluating several variables, including chemical composition, processing parameters, and ultrasonic measurements [17–19]. However, many current studies focus on small datasets or specialized materials, and comprehensive models that include mechanical properties, ultrasonic measurements, and process parameters remain scarce.

Therefore, for accurate *SG* iron casting evaluation, a methodical approach involving experimental design, ultrasonic characterization, and predictive modeling is needed. Using *Taguchi* experimental design and regression analysis, the present study aims to develop a non-destructive ultrasonic-based framework for predicting nodularity and mechanical properties of spheroidal graphite iron castings [20–21]. The ***objective*** is to establish clear relationships between ultrasonic velocity, nodularity, and mechanical properties, thereby making ultrasonic testing a useful tool for quality assessment in the *SG* iron foundry industry.

Methods

Three grades of spheroidal graphite (*SG*) iron – *SGI 400/12*, *SGI 500/7*, and *SGI 600/3* – that together offer a practical range of mechanical properties for engineering applications were the subject of the investigation [8–9]. The concentrations of carbon (*C*), silicon (*Si*), manganese (*Mn*), phosphorus (*P*), sulfur (*S*), magnesium (*Mg*), and copper (*Cu*, if present) are within the specified ranges of the respective *SG* iron standards, according to the actual chemical compositions of these grades, as displayed in Table 1 [22]. It has been determined that carbon, silicon, and phosphorus are very important in producing spheroidal graphite and, as a result, in regulating nodularity and mechanical behavior in the castings [22].

Table 1

Chemical composition of the *SG* iron grades

***SG* iron grade**	***C* (%)**	***Si* (%)**	***Mn* (%)**	***P* (%)**	***S* (%)**	***Mg* (%)**	***Cu* (%)**
400/12 (actual)	3.65	2.825	0.66	0.045	0.021	0.035	–
500/7 (actual)	3.45	2.62	0.45	0.045	0.018	0.035	0.4
600/3 (actual)	3.25	2.36	0.66	0.045	0.020	0.035	0.4

Designation: 400 – tensile strength (N/mm^2), 12 – elongation (%).

Experimental design and casting trials

Using the *Taguchi L27* orthogonal array, a methodical *Design of Experiments* (*DoE*) approach was employed to investigate the multifactorial impact of casting parameters on ultrasonic velocity and percentage nodularity in *SG* iron step castings. By examining three control factors at three levels each, the *L27* array efficiently covers the experimental domain. This preserves orthogonal balance and factor independence while reducing the number of trials from 81 (full factorial: 3^4) to 27 (full factorial: 3^3) [20]. Based on their known effects on graphite morphology and cooling behavior, three casting parameters were selected as control factors, as indicated in Table 2: (1) pouring temperature (***PT***) , which varies from 1,380 °C to 1,420 °C in 20 °C increments to modulate melt fluidity and solidification rate; (2) carbon equivalent (***CEV***), which ranges from 4.0 to 4.6 to investigate the impact of carbon content on graphite nucleation and growth; and (3) section thickness (***T***) , which varies from 5 mm to 15 mm to induce controlled variations in cooling rates and microstructural development [23].

Table 2

Input parameters and their levels for the *L27* orthogonal array

Parameter	**Designation**	**Level I**	**Level II**	**Level III**
Pouring temperature (°C)	***PT***	1,380	1,400	1,420
Carbon equivalent value	***CEV***	4.6	4.3	4.0
Section thickness (mm)	***T***	5	10	15

An induction furnace with a 500 kg capacity and medium frequency was used to produce the castings. Charge control and alloy additions were used to achieve the chemical composition of each nominal grade (*SGI 400/12*, *500/7*, and *600/3*); the measured compositions are displayed in Table 1. Green sand with a mean grain size of 0.25 mm, permeability of 250, and green strength of 1.8 MPa was used to create molds. At a rate of 0.4 wt.% of liquid metal, an inoculant material composed of ferrosilicon with strontium additions (typically 0.1% *Sr*) was applied. As the metal moved from the treatment ladle to the pouring ladle, the inoculation was applied, which caused the molten metal to dissolve quickly and distribute evenly. A thermocouple in the ladle was used to measure and record the pouring temperature at three distinct ***PT*** levels: 1,380; 1,400; and 1,420 °C. The duration of ambient cooling and mold shakeout for each casting was noted; samples were removed after the temperature reached ambient.

To enable systematic spatial analysis of process-property interactions throughout the entire parameter domain, all 27 experimental combinations listed in Table 3 were produced as step casting components in sand molds, with each casting consisting of three distinct thickness sections. Because of this geometric structure, all three thickness levels could be examined inside a single casting, reducing the mold preparation time and enabling a direct comparison of thickness effects under comparable pouring and composition conditions.

Table 3

***L27* orthogonal array**

Expt. No.	*PT* (°C)	*CEV*	T (mm)
1	1,380	4.6	5
2	1,380	4.6	10
3	1,380	4.6	15
4	1,380	4.3	10
5	1,380	4.3	15
6	1,380	4.3	5
7	1,380	4.0	15
8	1,380	4.0	5
9	1,380	4.0	10
10	1,400	4.6	5
11	1,400	4.6	10
12	1,400	4.6	15
13	1,400	4.3	10
14	1,400	4.3	15
15	1,400	4.3	5
16	1,400	4.0	15
17	1,400	4.0	5
18	1,400	4.0	10
19	1,420	4.6	5
20	1,420	4.6	10
21	1,420	4.6	15
22	1,420	4.3	10
23	1,420	4.3	15
24	1,420	4.3	5
25	1,420	4.0	15
26	1,420	4.0	5
27	1,420	4.0	10

Ultrasonic testing

Ultrasonic velocity (*UV*) in *SG* iron castings was measured using an *EEC*-made *ADVANSCAN AS-414* ultrasonic flaw detector with integrated analysis software. A 10 mm diameter, 4 MHz transducer probe was used to generate and receive ultrasonic waves. Equation (1) was used to calculate the ultrasonic velocity (***V***) as the ratio of the specimen thickness (***d***) to the wave's transit time (***t***) through the material:

$$V = \frac{d}{t}, \quad (1)$$

where the ultrasonic velocity depends on density, elasticity, and internal microstructural features [24–25].

After calibration, *SGI 400/12*, *SGI 500/7*, and *SGI 600/3* specimens were tested following a standardized procedure to ensure consistency [13–15]. Step casting specimens with section thicknesses of 5, 10, and 15 mm were evaluated as shown in Fig. 1 at predefined locations to capture the influence of geometry on *UV* and nodularity [26–27].

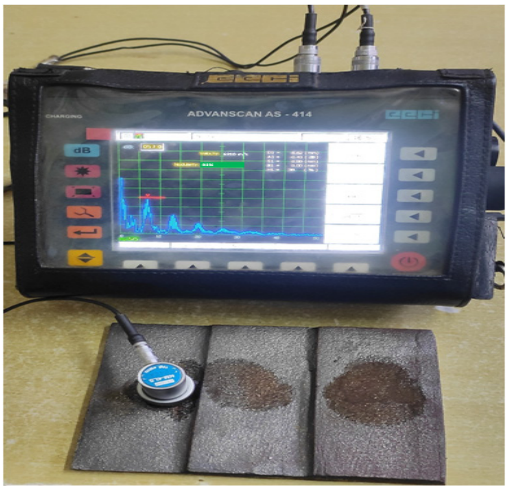

Fig. 1. Measurement of ultrasonic velocity and nodularity of the step casting

The percentage nodularity of ductile iron specimens was estimated using an *ADVANSCAN AS-414* ultrasonic flaw detector. By measuring the ultrasonic longitudinal wave velocity through a material with a predetermined thickness, the device indirectly evaluates nodularity. The ultrasonic pulse's time-of-flight is used to calculate the velocity, which is then compared to the device's internal calibration database. This database is based on previously established relationships between the microstructural characteristics of cast iron and ultrasonic velocity.

It is well known that graphite form, especially nodularity, has a significant influence on ultrasonic velocity in cast iron. Higher nodularity (spheroidal graphite) permits smoother wave propagation and higher velocities, while lower nodularity results in greater scattering and lower velocities. Consequently, the flaw detector uses previously established empirical relationships to map recorded velocity to nodularity values in order to determine nodularity. Similar trends have been found in previous research, confirming that graphite shape is the most important structural component influencing ultrasonic wave velocity in cast iron [28].

Tensile and hardness testing

Tensile and hardness tests were performed on specimens taken from the 5, 10, and 15 mm sections of the step castings corresponding to each *L27* experiment to assess mechanical behavior, as shown in Table 4. Tensile testing according to *ASTM E8/E8M* yielded ultimate tensile strength [29]. *Brinell* hardness measurements were performed in accordance with *ASTM E10* [30]. A 10 mm diameter steel ball indenter with an applied load of 3,000 kgf and a dwell time of 10–15 s was used for testing. For each specimen, three successive indentations were performed at different locations, and the reported hardness value represents the arithmetic mean of these measurements, for the purpose of correlating mechanical properties with process parameters and ultrasonic velocity [31–32].

Table 4

Tensile strength and hardness data of the step castings

Expt. No.	*PT* (°C)	*CEV*	Section thickness (mm)	Ultrasonic velocity (flaw detector, m/s)	% *N*	*UTS* (σ_u) (N/mm²)	Hardness
1	1,380	4.6	5	5,368	76	415	168
2	1,380	4.6	10	5,472	77	419	167
3	1,380	4.6	15	5,466	77	406	164
4	1,380	4.3	10	5,646	87	511	225
5	1,380	4.3	15	6,019	88	522	225
6	1,380	4.3	5	5,646	90	514	224
7	1,380	4.0	15	6,120	91	612	228
8	1,380	4.0	5	6,315	92	604	227
9	1,380	4.0	10	6,117	93.7	620	229
10	1,400	4.6	5	5,366	75	415	167
11	1,400	4.6	10	5,472	77	420	166
12	1,400	4.6	15	5,466	77	410	164

The End Table 4

Tensile strength and hardness data of the step castings

Expt. No.	*PT* (°C)	*CEV*	Section thickness (mm)	Ultrasonic velocity (flaw detector, m/s)	% *N*	*UTS* (σ_u) (N/mm²)	Hardness
13	1,400	4.3	10	5,646	89	511	225
14	1,400	4.3	15	6,019	88	517	222
15	1,400	4.3	5	5,646	90	527	226
16	1,400	4.0	15	6,120	92	621	232
17	1,400	4.0	5	6,315	93	613	231
18	1,400	4.0	10	6,117	93.7	623	230
19	1,420	4.6	5	5,366	75	416	169
20	1,420	4.6	10	5,472	77	422	168
21	1,420	4.6	15	5,466	77	409	165
22	1,420	4.3	10	6,019	88	516	226
23	1,420	4.3	15	6,019	89	522	227
24	1,420	4.3	5	5,646	91	526	226
25	1,420	4.0	15	6,120	92	619	233
26	1,420	4.0	5	6,315	93	612	230
27	1,420	4.0	10	6,117	93.7	628	231

Regression modelling

Multiple linear regression was used to create empirical predictive models that quantified the relationships between process parameters (pouring temperature (*PT*), carbon equivalent (*CEV*), section thickness (*T*)), ultrasonic velocity, and response variables (percentage nodularity, ultimate tensile strength (*UTS*, (σ_u)) , and *Brinell* hardness (*BHN*)). Models were fitted using the mean experimental values from all 27 trials, with no data preprocessing performed, allowing direct interpretation of coefficients in terms of process variables.

Nodularity model

A linear regression model for nodularity was developed based on the average ultrasonic velocity measurements ***V_f*** from the flaw detector and the corresponding nodularity data.

$$\%N = 230.2 + 0.0028PT - 30.23CEV + 0.029T - 0.00316V\_f\ , \quad (2)$$

where %*N* is the percentage nodularity; *PT* is the pouring temperature (°C); *CEV* is the carbon equivalent; *T* is the section thickness (mm); *V_f* is the ultrasonic velocity (m/s).

This model had an R^2 of 0.8955 and an adjusted R^2 of 0.8765, indicating a strong linear fit within the tested parameter range.

Tensile strength and hardness models

Similarly, *UTS* (σ_u) and hardness data from Table 4 were utilized to develop predictive models for tensile strength and *BHN* as a function of ***PT***, ***CEV***, ***T***, and ***V_f*** [1]. The resultant equations are:

$$UTS\ (\sigma_u) = 1,874 + 0.1306PT - 347.2CEV + 0.032T - 0.0082V\_f\ ; \quad (3)$$

$$BHN = 823 + 0.050PT - 131.8CEV + 0.103T - 0.0206V\_f\ , \quad (4)$$

where *BHN* represents *Brinell* hardness, while *UTS* (σ_u) is expressed in N/mm^2. The tensile strength model was quite accurate (R^2 = 0.9954 and adjusted R^2 = 0.9946), whereas the hardness model achieved R^2 = 0.8135 and adjusted R^2 = 0.7796, suggesting reasonable predictive capability for hardness within the experimental range [1].

Results and Discussion

Using quantifiable process and non-destructive parameters such as pouring temperature (***PT***), carbon equivalent (***CEV***), section thickness (***T***), and ultrasonic velocity (***V_f***), this study develops three regression models to predict important quality characteristics of ductile iron castings, including percentage nodularity (**%*N***), ultimate tensile strength (*UTS,* σ_u), and *Brinell* hardness (*BHN*). These models provide a coherent and practical framework for forecasting mechanical and microstructural characteristics without relying solely on destructive testing.

Model performance and statistical significance

All three models are significant and offer strong predictive potential, according to the statistical analysis. While the *BHN* model has a considerably lower but still outstanding R^2 = 81.35%, the **%*N*** and *UTS* (σ_u) models have substantial coefficients of determination (R^2 = 89.55% and 99.54%, respectively). Good model generalization and minimal overfitting are indicated by the predicted R^2 values closely matching the corresponding adjusted R^2 values [33]. Statistically significant regression models with ***P***-values less than 0.001 are shown in Tables 5–7. Strong correlations between input variables and responses that cannot be explained by random variation are indicated by high ***F***-values, particularly for the *UTS* (σ_u) model.

Table 5

Analysis of variance (*ANOVA*) for the nodularity (% *N*) model

Source	*DF*	*Adj SS*	*Adj MS*	*F*-value	*P*-value	% contribution
PT **(°C)**	2	14	7	7.78	0.003	1.12
CEV	2	1,185	592.5	658.33	0	94.46
T	2	16	8	8.89	0.002	1.28
V_f	2	8	4	4.44	0.027	0.64
Error	18	16.96	0.94	–	–	1.35
Total	26	1,254.96	–	–	–	100

Table 6

Analysis of variance (*ANOVA*) for the *UTS* (σ_u) model

Source	*DF*	*Adj SS*	*Adj MS*	*F*-value	*P*-value	% contribution
PT **(°C)**	2	1100	550	1.22	0.317	0.59
CEV	2	175,800	87,900	195.33	0	95.02
T	2	120	60	0.13	0.878	0.06
V_f	2	70	35	0.08	0.925	0.04
Error	18	7,922	440.1	–	–	4.28
Total	26	185,012	–	–	–	100

Table 7

Analysis of variance (*ANOVA*) for the for the *Brinell* hardness (*BHN*) model

Source	*DF*	*Adj SS*	*Adj MS*	*F*-value	*P*-value	% contribution
PT **(°C)**	2	55	27.5	1.1	0.354	0.24
CEV	2	21,450	10,725	429	0	94.79
T	2	45	22.5	0.9	0.423	0.20
V_f	2	25	12.5	0.5	0.614	0.11
Error	18	1,057.7	58.76	–	–	4.67
Total	26	22,632.7	–	–	–	100

Influence of process parameters

The most crucial factor in all three models is the carbon equivalent (***CEV***). With extremely low ***P***-values and high ***F***-values, it is statistically highly significant. The regression coefficients indicate a negative correlation between ***CEV*** and all responses (**%*N***, *UTS* (σ_u), and ***BHN***), suggesting that nodularity, tensile strength, and hardness decrease as ***CEV*** increases. This behavior is consistent with the principles of physical metallurgy. Higher ***CEV*** encourages increased graphite production, influences solidification behavior, reduces matrix hardness and strength, and alters graphite morphology [35]. Other variables — pouring temperature (***PT***), section thickness (***T***), and ultrasonic velocity (***V_f***) — have comparatively low individual statistical significance. Nevertheless, their inclusion improves the overall model accuracy, demonstrating that their combined effects significantly enhance property prediction.

Interaction effects between parameters

Interaction plots were examined to better understand the combined influence of variables. These graphs offer a deeper understanding of how two parameters interact to affect the response.

Relationship between ultrasonic velocity and CEV

An interaction plot between ultrasonic velocity and ***CEV*** is shown in Fig. 2, which reveals a distinct decreasing trend in ultrasonic velocity as ***CEV*** increases across all section thicknesses. This suggests that higher carbon equivalent results in poorer ultrasonic wave propagation. This phenomenon can be explained by microstructural differences. Higher ***CEV*** encourages increased graphite content and coarsening, which scatter ultrasonic vibrations and reduce velocity.

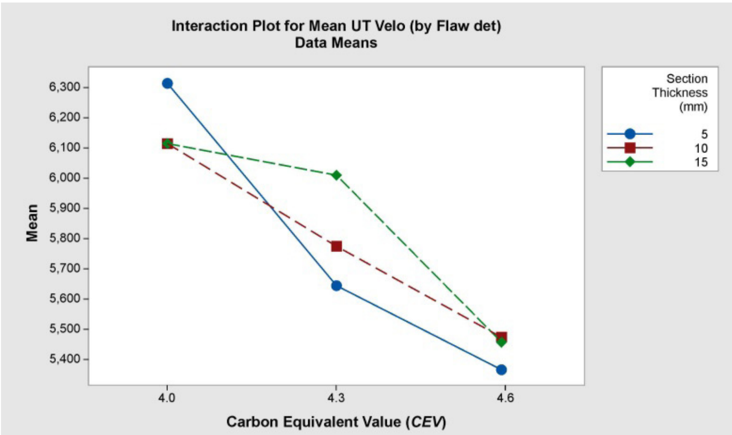

Fig. 2. Relation between ultrasonic velocity and *CEV*

Additionally, this trend is slightly modulated by changes in section thickness, indicating that cooling rate affects ultrasonic response. Thinner sections (which cool more quickly) exhibit comparatively higher velocities than thicker sections. This finding is consistent with previous studies showing that variations in the internal structure and graphite form of cast iron affect ultrasonic velocity [28, 34].

Relation between % nodularity and CEV

Nodularity clearly decreases as ***CEV*** increases, according to the interaction plot (Fig. 3) between **%*N*** and ***CEV***. This trend is consistent across all section thicknesses with only minor variations. High nodularity (>90%) and lower ***CEV*** values (~4.0), indicate favorable graphite spheroidization. However, nodularity sharply declines (to about 75–78%) as ***CEV*** increases (~4.6). This demonstrates that an excess of carbon equivalent negatively affects the formation of spherical graphite. Section thickness also influences this effect. At higher ***CEV*** values, thicker sections maintain slightly higher nodularity, most likely due to slower cooling rates that permit more stable graphite growth. Nevertheless, ***CEV*** still has a major detrimental effect. Higher carbon equivalent is linked to graphite shape degeneration and decreased nodularity as a result of altered solidification dynamics, providing strong evidence for this behavior [35].

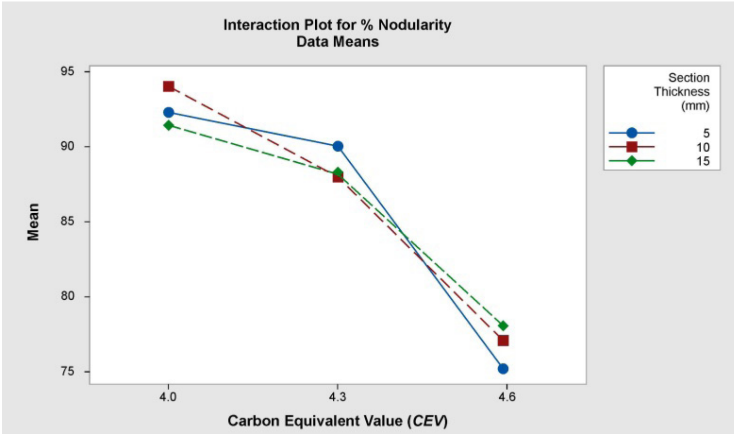

Fig. 3. Relation between % nodularity and *CEV*

Relation between % nodularity and pouring temperature

Pouring temperature has a moderate but discernible impact on nodularity, according to the interaction plot (Fig. 4) between percentage nodularity and pouring temperature. Nodularity is marginally increased at intermediate pouring temperatures (~1,400 °C), especially for medium section thickness. Nodularity tends to decrease or stabilize at lower temperatures (1,380 °C) and higher temperatures (1,420 °C). This demonstrates that optimal graphite spheroidization occurs within a specific range of pouring temperatures. Both excessively low and excessively high temperatures negatively affect nodule formation – low temperatures can cause premature solidification, while high temperatures can lead to magnesium treatment fading. The relationship with section thickness indicates that thicker sections are more susceptible to temperature variations, whereas thinner sections exhibit more consistent nodularity across temperature ranges. These results are due to variations in solidification times and cooling rates and are in line with the metallurgical understanding that pouring temperature significantly affects graphite nucleation and growth conditions [36].

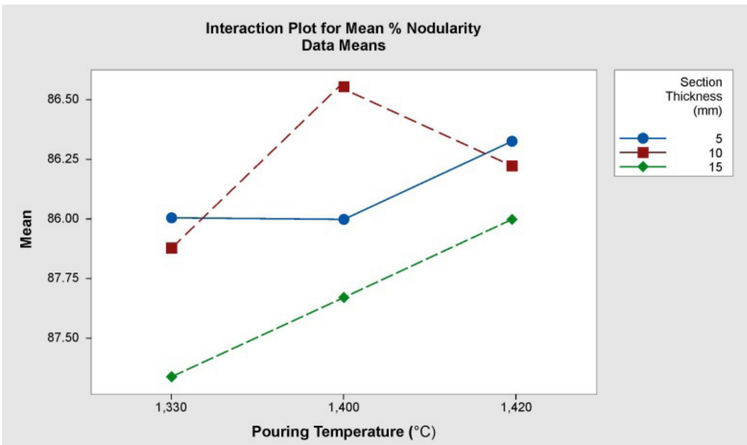

Fig. 4. Relation between % nodularity and pouring temperature

Microstructural validation and agreement analysis

Microstructural validation of representative *SG* iron samples was performed using an inverted metallurgical microscope at 100× magnification. The microstructural analysis was conducted on nine representative samples that included all combinations of three *SG* iron grades (*SGI 400/12*, *500/7*, and *600/3*) and three section thicknesses (5 mm, 10 mm, and 15 mm). For metallographic analysis, samples from each grade were sectioned from the cast specimens, mounted, polished, and etched according to *ASTM A247*. The microstructure was examined using an optical microscope, and digital micrographs were taken. The micrographs were then processed with image analysis software to calculate the percentage of spheroidal graphite particles relative to the total graphite area, which corresponds to the percentage nodularity defined in ASTM A247 [37].

The validation dataset in Table 8 shows a high correlation between ultrasonic nodularity estimations from the *ADVANSCAN AS-414* flaw detector and optical microscopy at 100× magnification. Ultrasonic nodularity values of 76–77% for the SGI 400/12 grade at ***CEV*** 4.6 were very close to metallographic values of 75.33–78%, with a maximum divergence of 2%. At moderate ***CEV*** 4.3 (*SGI 500/7*), ultrasonic nodularity of 89–90% was consistent with microscopic nodularity of 87.34–89%, again within a maximum divergence of 2–3% range. At the lowest ***CEV*** 4.0 (*SGI 600/3*), ultrasonic nodularity of 92–94% matched metallographic values of 91.33–94%, with only slight variability.

Table 8

Validation of nodularity: ultrasonic testing and optical microscopy

SG **iron grade**	***CEV***	**Thickness (mm)**	**Ultrasonic velocity (m/s)**	**Ultrasonic % *N***	**Microscopic % *N***
400/12	4.6	5	5,363	76	75.33
400/12	4.6	10	5,470	77	77
400/12	4.6	15	5,470	77	78
500/7	4.3	5	5,645	90	87.34
500/7	4.3	10	5,645	89	88.33
500/7	4.3	15	6,018	89	89
600/3	4.0	5	6,315	93	91.33
600/3	4.0	10	6,114	94	92.33
600/3	4.0	15	6,114	92	94

Microstructural examination (Fig. 5, 100× magnification, 2% nital etch) shows that lower ***CEV*** (*SGI 600/3*) results in well-defined, uniformly distributed spheroidal graphite particles within a continuous metallic matrix, whereas higher ***CEV*** (*SGI 400/12*) results in irregular, non-spheroidal graphite morphology with matrix discontinuities. These optical studies validate the quantitative relationships revealed by ultrasonic velocity and regression analysis, with nodularity variations (*SGI 600/3*: 92–94%, *SGI 400/12*: 74–78%), which are directly reflected in both microscopic morphology and acoustic propagation behavior. Despite minor differences in measurement principles, the statistical analysis confirms a linear relationship between nodularity and ultrasonic velocity, with higher velocities consistently associated with higher nodularity percentages, reinforcing ultrasonic velocity's utility as a quantitative indicator of microstructural quality.

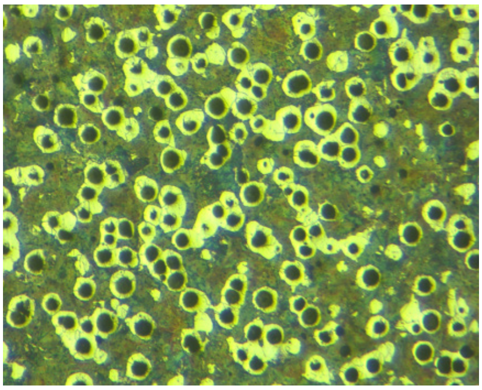

a

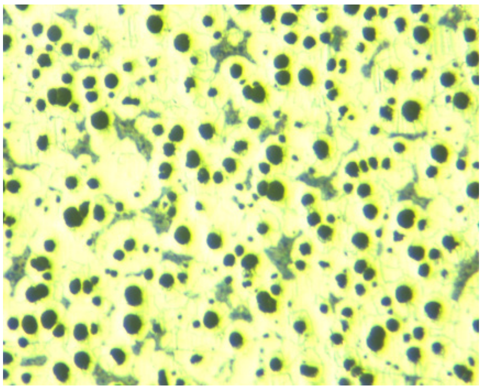

b

Fig. 5. Microstructures of 600/3 (*a*) and 400/12 (*b*) etched with 2% nital solution (captured using inverted microscope at 100× magnification)

Conclusion

1. This study discovered a substantial relationship between graphite nodularity and ultrasonic velocity in *SG* iron castings produced under controlled conditions. The investigation covered a wide range of parameters (*PT* 1,380–1,420 °C, *CEV* 4.0–4.6, *T* 5–15 mm) and three commercially important cast iron grades (*SGI 400/12*, *SGI 500/7*, and *SGI 600/3*).

2. Based on process parameters and ultrasonic velocity, the study developed regression models to forecast nodularity, *UTS* (σ_u), and *BHN*. The models show excellent agreement with experimental results and high forecast accuracy.

3. The carbon equivalent (*CEV*) was shown to be the most significant factor. *CEV* plays a crucial role in microstructure regulation, since interaction plots showed that it has a significant impact on both nodularity and ultrasonic velocity.

4. Using ultrasonic velocity for non-destructive prediction offers an effective real-time quality control method. Because these models are straightforward and efficient, they are highly beneficial for small-scale foundries.

A key contribution is the inclusion of ultrasonic velocity (***V_f***) in all models. Internal characteristics including microstructure, density, and elastic properties are detectable by ultrasonic examination. By combining ***V_f*** with process parameters, the models may predict nodularity, hardness, and tensile strength non-destructively. This enhances real-time quality assessment while eliminating the need for destructive testing. Significant relationships between ultrasonic parameters and material properties in cast irons have also been discovered in earlier studies [28, 34]. Since small-scale foundries have limited access to contemporary testing facilities, the suggested models are particularly helpful. Section thickness, chemical composition (for *CEV*), pouring temperature, and ultrasonic velocity are all routinely recorded or easily measurable. Operators can predict important material qualities with ease by integrating these models into basic tools like spreadsheets or mobile devices. This enables: real-time process control, rapid quality assessment, reduced testing costs, and prompt corrective action. This predictive ability improves casting quality consistency and efficiency.

Limitations and future work

The linear regression models are strictly calibrated to the examined parameter space (CEV 4.0–4.6, PT 1380–1420 °C, T 5–15 mm) and should not be extrapolated beyond these boundaries without additional validation. Factors such as microstructural heterogeneity, inoculation practice variations, and mold material differences – which were not varied in this study – may influence production performance and warrant future investigation. Nevertheless, the demonstrated methodology provides a rigorous, scalable framework for advancing non-destructive quality control in *SG* iron manufacturing and supporting evidence-based process optimization.

References

1. Sangame B.B., Reddy Y.P. Investigation on effect of different types of inoculants on the solidification of ductile cast iron using thermal analysis. *Multidiscipline Modeling in Materials and Structures*, 2024, vol. 20 (6), pp. 995–1012. DOI: 10.1108/MMMS-03-2024-0084.

2. Benini L., de Paula P.P.R., Tavares S.S.M., de Sá Carnerio F., Noris L.F., da Conceição B.M., Júnior J.M.M. Evaluation of austempered ductile iron end milling by magnetic Barkhausen noise and x-ray diffraction methods. *Journal of Materials Engineering and Performance*, 2025, vol. 34, pp. 9026–9036. DOI: 10.1007/s11665-025-10794-6.

3. Mohan H.K.C., Devaraj S., Swamy K.S.N., Venkatesh B.K. Microstructure and tribological property correlations of die cast and spray formed Al-30 wt.% Si alloy. *Journal of Mines, Metals and Fuels*, 2022, vol. 70 (10A), pp. 307–313. DOI: 10.18311/jmmf/2022/32772.

4. Kadam S., Kabnure B., Mhamane D. Computer-aided simulation of railway insert for defect analysis and yield improvement. *Journal of the Institution of Engineers (India): Series C*, 2021, vol. 102, pp. 651–656. DOI: 10.1007/s40032-021-00680-0.

5. Freitas V.L. de A., De Albuquerque V.H.C., Silva E. de M., Silva A.A., Tavares J.M.R.S. Nondestructive characterization of microstructures and determination of elastic properties in plain carbon steel using ultrasonic measurements. *Materials Science and Engineering: A*, 2010, vol. 527 (16–17), pp. 4431–4437. DOI: 10.1016/j.msea.2010.03.090.

6. Nanekar P.P., Shah B.K. Characterization of material properties by ultrasonic. *BARC Newsletter*, 2003, no. 249, pp. 25–38.

7. Toozandehjani M., Matori K.A., Ostovan F., Mustapha F., Oskoueian A. On the correlation between microstructural evolution and ultrasonic properties: A review. *Journal of Materials Science*, 2015, vol. 50 (7), pp. 2643–2665. DOI: 10.1007/s10853-015-8855-x.

8. Kim S.A., Johnson W.L. Elastic constants and internal friction of martensitic steel, ferritic-pearlitic steel, and α-iron. *Materials Science and Engineering: A*, 2007, vol. 452–453, pp. 633–639. DOI: 10.1016/j.msea.2006.11.147.

9. Kumar A., Jayakumar T., Raj B. Influence of precipitation of intermetallics on Young's modulus in nickel and zirconium base alloys. *Philosophical Magazine Letters*, 2006, vol. 86 (9), pp. 579–587. DOI: 10.1080/09500830600936401.

10. Lévesque D., Kruger S.E., Lamouche G., Kolarik R., Jeskey G., Choquet M., Monchalin J.-P. Thickness and grain size monitoring in seamless tube making process using laser ultrasonics. *NDT & E International*, 2006, vol. 39 (8), pp. 622–626. DOI: 10.1016/j.ndteint.2006.04.009.

11. Badidi Bouda A., Benchaala A., Alem K. Ultrasonic characterization of materials hardness. *Ultrasonics*, 2000, vol. 38 (1–8), pp. 224–227. DOI: 10.1016/S0041-624X(99)00081-5.

12. Aghaie-Khafri M., Honarvar F., Zanganeh S. Characterization of grain size and yield strength in AISI 301 stainless steel using ultrasonic attenuation measurements. *Journal of Nondestructive Evaluation*, 2012, vol. 31 (3), pp. 191–196. DOI: 10.1007/s10921-012-0134-z.

13. Vasudevan M., Palanichami P. Characterization of microstructural changes during annealing of cold worked austenitic stainless steel using ultrasonic velocity measurements and correlation with mechanical properties. *Journal of Materials Engineering and Performance*, 2002, vol. 11 (2), pp. 169–179. DOI: 10.1361/105994902770344231.

14. Jodhani J., Handa A., Gautam A., Rana R. Ultrasonic non−destructive evaluation of composites: A review. *Materials Today: Proceedings*, 2023, vol. 78, pp. 627–632. DOI: 10.1016/j.matpr.2022.12.055.

15. Belan J., Tillová E., Uhríčik M., Pastierovičová L. Influence of structural parameters – the shape of graphite and matrix on change of ultrasonic wave propagation rate and value of attenuation in graphitic cast irons. *Production Engineering Archives*, 2023, vol. 29 (1), pp. 23–27. DOI: 10.30657/pea.2023.29.4.

16. Hütter S., Lafarge R., Simonin J., Mook G., Brosius A., Halle T. Determination of microstructure changes by eddy-current methods for cold and warm forming applications. *Advances in Industrial and Manufacturing Engineering*, 2021, vol. 2, p. 100042. DOI: 10.1016/j.aime.2021.100042.

17. Hatate M., Nobuki T., Komatsu S. Accuracy improving methods in estimation of graphite nodularity of ductile cast iron by measurement of ultrasonic velocity. *Science and Technology of Casting Processes*. InTech, 2012. DOI: 10.5772/50596.

18. Agnoletto D., Lemos G.V., Beskow A.B., Lessa C.R., Reguly A. Methodology for determination of degree of nodularity in a ductile cast iron GGG 40 by ultrasonic velocity test. *Southern Brazilian Journal of Chemistry*, 2018, vol. 26, pp. 10–16. DOI: 10.37633/SBJC.26(26)2018.10-16.

19. Yadav A., Prajapati K.K., Mitra M. Deep learning-assisted prediction of mean grain size of polycrystalline materials from ultrasonic wave response. *Mechanics of Materials*, 2025, vol. 207, p. 105367. DOI: 10.1016/j.mechmat.2025.105367.

20. Yusubov F. Wear studies on phenolic brake-pads using Taguchi technique. *Tribology in Industry*, 2021, vol. 43, pp. 489–499. DOI: 10.24874/ti.1024.12.20.03.

21. Kabnure B.B., Shinde V.D., Kolhapure R.R. Optimization to develop multiple response microstructure and hardness of ductile iron casting by using GRA. *Journal of the Institution of Engineers (India): Series D*, 2018, vol. 99, pp. 235–243. DOI: 10.1007/s40033-018-0161-8.

22 Regordosa A., Llorca-Isern N., Sertucha J., Lacaze J. Evolution of shrinkage with carbon equivalent and inoculation in ductile cast irons. *Materials Science Forum*, 2018, vol. 925, pp. 28–35. DOI: 10.4028/www.scientific.net/MSF.925.28.

23. Brown J.R. *Foseco ferrous foundryman's handbook*. 10th ed. Butterworth-Heinemann, 2000.

24. McDonald M., Gaines S., Diederichs M. Interpreting ultrasonic pulse velocities and elastic properties of lac du bonnet granite under compression. *IOP Conference Series: Earth and Environmental Science*, 2023, vol. 1124, p. 012035. DOI: 10.1088/1755-1315/1124/1/012035.

25. Muthmari S., Singh A. Review of various ultrasonic techniques employed in modern industries. *International Journal of Engineering Science and Technology*, 2011, vol. 3, pp. 3078–3085.

26. Maggi L.E., Silva C.E.R., Alvarenga A.V., Costa-Felix R.P.B. Ultrasonic calibration and certification of V1 and V2 type reference standard blocks for use in non-destructive testing. *Journal of Physics Conference Series*, 2011, vol. 279 (1), p. 012029. DOI: 10.1088/1742-6596/279/1/012029.

27. Pitkänen J., Sarkimo M., Lonne S. Modeling of ultrasonic testing for inspection of nodular cast iron insert. *6th International Conference on NDE in Relation to Structural Integrity for Nuclear and Pressurized Components*, Budapest, Hungary, 2007. Available at: https://www.ndt.net/search/docs.php3?id=7016 (accessed 09.04.2026).

28. Lee S.-C., Suen J.-M. Ultrasonic nondestructive evaluation of matrix structures and nodularity in cast irons. *Metallurgical Transactions A*, 1989, vol. 20A, pp. 2399–2407. DOI: 10.1007/BF02666675.

29. ASTM E8/E8M-16a: *Standard test methods for tension testing of metallic materials*. ASTM International, 2020. DOI: 10.1520/E0008_E0008M-16A.

30. ASTM E10-18: *Standard test method for Brinell hardness of metallic materials*. ASTM International, 2023. DOI: 10.1520/E0010-18.

31. Mhamane D., Bewoor A. A non-destructive approach to characterize nodularity in SG iron castings using ultrasonic testing. *Journal of Mines, Metals and Fuels*, 2025, vol. 73 (11), pp. 3589–3598. DOI: 10.18311/jmmf/2025/50001.

32. Mhamane D.A., Bewoor A.K., Mhamane R.D., Bewoor L.A. *Process for predicting nodularity, material properties in SG iron castings using simulation and ultrasonic testing*. Patent No. 202521031317, 2025.

33. Montgomery D., Cahyono St. *Design and analysis of experiments*. 9th ed. John Wiley & Sons, 2022.

34. Gür C.H., Aydinmakina B. Ultrasonic investigation of graphite nodularity in ductile cast irons. *DGZfP Jahrestagungen 2001. ZfP in Anwendung, Entwicklung und Forschung*, Berlin, 21–23 Mai, 2001. Available at: https://www.ndt.net/article/dgzfp01/papers/p33/p33.htm (accessed 07.04.2026).

35. Stefanescu D.M. *Science and engineering of casting solidification*. 2nd ed. Springer, 2015. DOI: 10.1007/978-3-319-15693-4.

36. Campbell J. *Complete casting handbook*. 2nd ed. Butterworth-Heinemann, 2015. DOI: 10.1016/C2014-0-01548-1.

37. ASTM A247-19: *Standard test method for evaluating the microstructure of graphite in iron castings*. ASTM International, 2024. DOI: 10.1520/A0247-19. Available at: https://store.astm.org/a0247-19.html (accessed 09.04.2026).

Conflicts of Interest

The authors declare no conflict of interest.